



A new multiscale formulation for the electromechanical behavior of nanomaterials

Harold S. Park^{a,*}, Michel Devel^b, Zhao Wang^c

^a Department of Mechanical Engineering, Boston University, Boston, MA 02215, United States

^b Institut FEMTO-ST, Université de Franche-Comté, CNRS, ENSMM, UTBM, 26 chemin de l'épitaphe, F-25030 Besançon Cedex, France

^c LITEN, CEA-Grenoble, 17 rue des Martyrs, 38054 Grenoble Cedex 9, France

ARTICLE INFO

Article history:

Received 26 November 2010

Received in revised form 29 March 2011

Accepted 4 April 2011

Available online 12 April 2011

Keywords:

Surface Cauchy–Born

Electromechanical coupling

Gaussian dipole model (GDM)

Finite elements

Surface stress

Point dipole interaction (PDI) model

ABSTRACT

We present a new multiscale, finite deformation, electromechanical formulation to capture the response of surface-dominated nanomaterials to externally applied electric fields. To do so, we develop and discretize a total energy that combines both mechanical and electrostatic terms, where the mechanical potential energy is derived from any standard interatomic atomistic potential, and where the electrostatic potential energy is derived using a Gaussian-dipole approach. By utilizing Cauchy–Born kinematics, we derive both the bulk and surface electrostatic Piola–Kirchhoff stresses that are required to evaluate the resulting electromechanical finite element equilibrium equations, where the surface Piola–Kirchhoff stress enables us to capture the non-bulk electric field-driven polarization of atoms near the surfaces of nanomaterials. Because we minimize a total energy, the present formulation has distinct advantages as compared to previous approaches, where in particular, only one governing equation is required to be solved. This is in contrast to previous approaches which require either the staggered or monolithic solution of both the mechanical and electrostatic equations, along with coupling terms that link the two domains. The present approach thus leads to a significant reduction in computational expense both in terms of fewer equations to solve and also in eliminating the need to remesh either the mechanical or electrostatic domains due to being based on a total Lagrangian formulation. Though the approach can apply to three-dimensional cases, we concentrate in this paper on the one-dimensional case. We first derive the necessary formulas, then give numerical examples to validate the proposed approach in comparison to fully atomistic electromechanical calculations.

© 2011 Elsevier B.V. All rights reserved.

1. Introduction

Developing a fundamental understanding of how nanomaterials deform and respond mechanically to externally applied electromagnetic fields will be critical to advancing various aspects of nanoscale science and engineering. For example, recent research has shown that carbon nanotubes exhibit giant electrostriction [1,2], in which the nanotubes show significant electromechanical energy conversion potential by undergoing extremely large deformations in response to an applied electric field. Furthermore, many nanoelectromechanical systems (NEMS), which are used for a wide range of applications including force [3], displacement [4,5] and mass [6,7] sensing, are actuated by means of external electromagnetic fields [7,8]. Finally, electric fields are also used by experimentalists to grow and align nanostructures [9], to drive nanostructures to resonance to measure their size-dependent elastic properties [10,11], and also to deform nanostructures in order

to examine the instability and failure mechanisms that occur with increasing deformation [1,12–14].

The multiphysics computational modeling of electromechanical phenomena has focused in recent years on developing techniques to study microelectromechanical systems (MEMS). A common approach to this problem has been to utilize an electrostatic analysis to compute the electrostatic forces, while a mechanical analysis is required to compute the deformation of the structure in response to the applied electrostatic forces. The semi-Lagrangian approach is a common technique for solving the coupled electromechanical system of equations in which the mechanical analysis is performed using the finite element method (FEM) in the undeformed configuration using a Lagrangian description [15–17], while the boundary element method (BEM) is typically used to perform the electrostatic analysis on the deformed geometry. Self-consistency between the mechanical and electrostatic simulations is achieved using relaxation techniques [18]. However, these approaches also have certain deficiencies; these include the fact that the geometry of the structure must be remeshed before an electrostatic analysis is performed [19]; the BEM interpolation functions must be recalculated during each relaxation iteration [20]; convergence rates for

* Corresponding author.

E-mail address: parkhs@bu.edu (H.S. Park).

the coupled analysis using the relaxation scheme can falter when deformations of the mechanical domain are large [20]. These issues can be alleviated using the recently developed full Lagrangian approach of Aluru et al. [18,20–22]; however, this approach still requires the implicit and coupled solution of both the mechanical and electrostatic equations, as well as the calculation of the electromechanical coupling matrices, leading to considerable computational expense, particularly for 3D problems. We note that other approaches, including Lagrange multiplier-based staggered techniques for solving the coupled electromechanical system of equations [23,24], also require the solution of both the mechanical and electrostatic governing equations in addition to electromechanical coupling terms.

Moreover, there are additional challenges that must be overcome to extend the previously discussed computational electromechanical techniques for MEMS down to the nanoscale; these challenges pertain to capturing the appropriate surface physics that occur in either the mechanical or electrostatic domains. For example, due to nanoscale surface effects [25] that arise from the undercoordinated nature of atomic bonding at surfaces, the mechanical properties of nanostructures have been shown both experimentally [10,26–29] and theoretically [30–34] to deviate from the expected bulk values, particularly when the characteristic size of the nanostructure decreases below 50 nm [26].

In addition to the surface effects on the mechanical properties of nanostructures, atoms that lie at surfaces respond, and in particular polarize differently due to applied electric fields as compared to atoms that lie within the material bulk. While this has not been studied extensively in the literature, recent atomistic calculations have found that surface atoms for various materials exhibit a significantly different polarizability in response to applied electric fields [35–38] as compared to bulk atoms.

Therefore, there are two major objectives for the present work. First, we wish to significantly reduce the computational expense of analyzing coupled electromechanical problems by solving only one governing equation, rather than equations for both the mechanical and electrostatic domains. Second, we wish to incorporate the appropriate surface-driven mechanical and electrostatic physical phenomena into our computational model. To accomplish the first task, we follow the recent developments of Wang et al. [39,40], who, within a fully atomistic context, used an atomistic total energy that combined both mechanical and electrostatic energies. In their approach, the mechanical potential energy was obtained from the AIREBO interatomic potential for carbon [41], while the electrostatic potential energy in response to an external electrostatic field was obtained from either the Gaussian dipole [42,43] (for semiconducting nanostructures) or Gaussian charge-dipole [44,45] (for metallic nanostructures) approaches. In these papers [39,40], the self-consistent calculation of the effective charges, dipoles, energies and electrostatic forces on every atom at each iteration was made computationally tractable through analytic expressions that involved the inversion of a single matrix, thus eliminating the need for numerical derivations to compute the forces. Indeed, this allowed them to find equilibrium positions by minimizing the total atomistic potential energy fully self-consistently with a single total energy functional.

To accomplish the second task, we build upon previous work by Park et al. [46–48], who developed an extension to Cauchy–Born techniques called the surface Cauchy–Born (SCB) model to capture the non-bulk mechanical surface energies of nanostructures within a continuum, FEM-based computational methodology. The SCB model was previously shown to accurately capture nanoscale surface stress effects on the mechanical behavior and properties of both FCC metallic [34,47,49] and semiconducting (silicon) [50,51] nanowires as compared to benchmark fully atomistic calculations.

The major result of this article is then a multiscale, finite deformation FEM-based methodology that enables us to study how surface-dominated nanostructures respond to externally applied electric fields. For the sake of clarity we restrict this first paper to one dimensional (1D) systems and reserve the full 3D formalism for a subsequent paper, which follows the same lines of development but with some complications due to the tensor formalism. We therefore begin by developing the total atomistic potential energy for 1D systems, then arrive at a single governing electromechanical finite element equation that captures external electric field effects on nanostructures. We further derive from the Gaussian dipole model of electrostatics, using Cauchy–Born kinematics, the bulk and surface electrostatic Piola–Kirchhoff stresses that are required for the coupled electromechanical finite element governing equations. Our numerical examples in 1D validate both the bulk electrostatic stress, and also the surface electrostatic stress by comparison to fully coupled electromechanical atomistic simulations.

2. Atomistic electromechanical potential energy

We briefly describe in this section the atomistic electromechanical potential energy that was previously developed by Wang and Devel [39,40] to study the effect of an external electrostatic field on the deformation of semiconducting and metallic carbon nanotubes. Specifically, they wrote the total energy of the nanostructure as the sum of the mechanical and electrostatic energies as:

$$U^{total}(r_{ij}) = \sum_{i=1}^N U_i^{elec}(r_{ij}) + \sum_{i=1}^N U_i^{mech}(r_{ij}), \quad (1)$$

where N is the total number of atoms in the system and r_{ij} is the distance between two atoms i and j . In their approach, the mechanical potential energy U^{mech} was obtained using a standard interatomic potential, i.e. the AIREBO potential for carbon [41], while the supplementary electrostatic potential energy U^{elec} due to an externally applied electric field was obtained using either the Gaussian dipole-only model for semiconducting carbon nanotubes (CNTs) [39] or the Gaussian charge-dipole model for metallic CNTs [40], which we will discuss in further detail in the next section. It is worth noting that there are no restrictions on the choice of the mechanical interatomic potential as long as it accurately represents the behavior of the material to be studied in the absence of an externally applied electric field. The minimum energy configuration (i.e. the mechanical deformation) of the nanotubes in the presence of the externally applied electric field was then obtained by direct minimization of the total energy (1).

Because the calculation of mechanical interatomic forces is routinely done in the literature, we will not overview that here, and instead refer the reader to classic texts on molecular simulation [52,53]. However, the analytical calculation of electrostatic forces from the Gaussian dipole model has been much less publicized. We will therefore discuss it in the next chapter, emphasizing the aspects of computational difficulty and expense that motivate the present work.

3. Atomistic electrostatic potential energy: Gaussian dipole method

3.1. Background

In this section, we describe the theory underlying the calculation of the atomistic electrostatic potential energy arising in response to an external field via the Gaussian dipole model (GDM), and provide motivation for why it is critical to develop computationally efficient, multiscale techniques for calculating

the electrostatic stress. The GDM can be viewed as an extension of the point dipole interaction model (PDI), which was originally developed as a semi-phenomenological model to describe the interaction of matter at the atomistic scale with an external electric field [54–57]. This model simply states that the response of a dielectric to an externally applied field can be described to first order by the fact that the nuclei and electrons are attracted in opposite directions. Hence the macroscopic polarization of the material is accounted for by the creation of elementary dipoles on every atoms. The total field on a given atom is then computed self-consistently by stating that it is the sum of the external field plus the fields created by the other dipoles which are themselves created by the total fields at their positions. Furthermore, the (mesoscopic) discretization of the volume integrals occurring in electromagnetic waves scattering by finite objects leads to the same kind of equations, so that this method has been used in many branches of science with so many variants bearing different names that we can give only examples here: astrophysics [58,59], where it is known as the discrete dipole approximation (DDA), local probe microscopies where it is known as the generalized field susceptibility technique [60,61] or electric field propagators (EFP) technique [62] or Green's dyadic function technique as in other domains of electromagnetism [63], biophysics and organic molecular simulations [64–68].

The fact that the PDI/DDA model has been successful across this range of length scales, from atoms to interstellar dust grains, indicates its robustness and physical correctness. It is however, only a special case of a more general multipolar approach [60,69,70]. Indeed, for metallic materials or organic molecules with delocalized electrons coming from conjugated double bounds, a charge + dipole model is better suited [44,45,71,72]. However, in all of these models, there are numerical difficulties coming from the self-energy of the atoms and the fact that when atoms are too closely bound, the point charge or dipole approximation is not a good approximation for nearest neighbors, leading to so-called 'polarization catastrophes'. Several techniques have been developed to avoid these divergences [43–45,72–77], which allowed one to consider metallic and semiconducting nanostructures including carbon nanotubes [14,45,78–80] and small metallic [36,38] and silicon nanoclusters [35]. Among them, the Gaussian dipole model (GDM) simply states that the interaction of the atoms with an external field does not create point dipoles but Gaussian dipoles, i.e. dipoles created from the shift of Gaussian distributions of charges. This results in interaction tensors between dipoles which are the convolution of the classical gradients of Green's function for Poisson's equation by one [43] or two [44] Gauss normalized distributions. This is in fact very similar to the Gaussian orbitals used in quantum chemistry and to the spatial part of the Ewald summation method for dipoles [81], and requires only knowledge of the deformed atomic positions to calculate the induced dipole moments p_i on each atom due to an external electric field E_0 .

3.2. Computation of the dipoles, energies and forces

In 1D, according to the GDM, the electrostatic potential energy U^{elec} corresponding to the response of the system to an external field can be written as, for a system of N atoms that has zero net charge (i.e. a semiconductor):

$$U^{elec} = \left(-\frac{1}{2} \sum_{i=1}^N \sum_{j=1}^N p_i T^{(2)}(r_{ij}) p_j \right) - \sum_{i=1}^N p_i E_0(r_i), \quad (2)$$

where E_0 is the externally applied electric field (in units of V/Å), p_i is the dipole moment for atom i (homogeneous to a charge multiplied by a distance), ϵ_0 is the permittivity of free space, and where $T^{(2)}$ is the Gaussian dipole – Gaussian dipole interaction tensor.

The 1D vacuum dipole–dipole interaction tensor $T_0^{(2)}$ is obtained from Equation (A3) of Langlet et al. [43] or Eq. (3) of Mayer [45] (with $a_{ij} = \sqrt{R_i^2 + R_j^2} = \sqrt{2}R$ if all atoms are of the same chemical nature):

$$T_{ij}^{(2)} = \frac{2}{(4\pi\epsilon_0)r_{ij}^3} \left(\operatorname{erf}\left(\frac{r_{ij}}{a_{ij}}\right) - \frac{2}{\sqrt{\pi}} \frac{r_{ij}}{a_{ij}} \left(1 + \frac{r_{ij}^2}{a_{ij}^2} \right) \exp^{-\left(r_{ij}/a_{ij}\right)^2} \right), \quad (3)$$

where $T_{ij}^{(2)} = T^{(2)}(r_{ij})$. Thanks to the convolution with the Gaussian (s), the quantities $T_{ii}^{(2)}$ are well defined ($T_{ii}^{(2)} = -1/((3\pi\epsilon_0)\sqrt{\pi}a_{ij}^3)$), which is not the case for the classical point dipole – point dipole propagator $-\nabla\nabla'(1/(4\pi\epsilon_0|\mathbf{r} - \mathbf{r}'|))$ which diverges when $|\mathbf{r} - \mathbf{r}'| \rightarrow 0$. Indeed, coupled with the crucial remark by Mayer [72] that the diagonal terms $-(1/2)p_i T_{ii}^{(2)} p_i$ should be included in the sum of Eq. (2) and physically interpreted as the self-energy of the atom $(1/2)\alpha_i E_i^2 = (1/2)p_i^2/\alpha_i$, the isotropic polarizability is related to the width of the Gaussian distribution of charge on each atom by Eq. (2) of Mayer et al. [44], and takes the form:

$$\frac{\alpha_i}{4\pi\epsilon_0} = 3 \frac{\sqrt{\pi}}{4} a_{ii}^3 = 3 \sqrt{\frac{\pi}{2}} R_i^3, \quad (4)$$

where R_i is the width of the Gaussian distribution for atom i , with units of Å, if $\alpha_i/(4\pi\epsilon_0)$ is given in Å³ as is commonly the case (which enables one to forget the factor $(4\pi\epsilon_0)$ in $T^{(2)}$ and fall back to the CGS–Gauss expression for it).

The distribution of dipoles is then determined by enforcing that the actual dipole distribution $\{p_j^*\}$ should correspond to the minimum value of U^{elec} . Following Wang et al. [39], this can be written as:

$$\forall i = 1, \dots, N \quad \frac{\partial U^{elec}}{\partial p_i} \left(\{p_j^*\} \right) = 0. \quad (5)$$

Enforcing these conditions on Eq. (2), the actual dipole moments on each atom p_j^* can be found by solving the following dense linear system:

$$\forall i = 1, \dots, N \quad \sum_{j=1}^N T_{ij}^{(2)} p_j^* = -E_{0,i}, \quad (6)$$

where $E_{0,i} = E_0(r_i)$. One can then define a $N \times N$ matrix $\widehat{T}^{(2)}$ and the corresponding vectors \widehat{p}^* and \widehat{E}_0 and restate the linear system to solve as:

$$\widehat{T}^{(2)} \widehat{p}^* = -\widehat{E}_0. \quad (7)$$

By substituting (6) into (2), one gets:

$$U^{elec} = -\frac{1}{2} \sum_{i=1}^N p_i^* (-E_{0,i}) - \sum_{i=1}^N p_i^* E_{0,i} = -\frac{1}{2} \sum_{i=1}^N p_i^* E_{0,i} = -\frac{1}{2} \widehat{p}^* \cdot \widehat{E}_0. \quad (8)$$

Using Eqs. (8) and (6) in its matrix form, the electrostatic forces on each atom can be written as:

$$\forall i = 1, \dots, N \quad f_i^{elec} = -\frac{\partial U^{elec}}{\partial r_i} = \frac{dE_0(r_i)}{dr_i} p_i^* - \frac{1}{2} \widehat{E}_0 \cdot \frac{\partial \left[\widehat{T}^{(2)} \right]^{-1}}{\partial r_i} \widehat{E}_0, \quad (9)$$

Then, using the fact that:

$$\frac{\partial \left\{ \widehat{T}^{(2)} \left[\widehat{T}^{(2)} \right]^{-1} \right\}}{\partial r_i} = 0 \Rightarrow \frac{\partial \left[\widehat{T}^{(2)} \right]^{-1}}{\partial r_i} = - \left[\widehat{T}^{(2)} \right]^{-1} \frac{\partial \widehat{T}^{(2)}}{\partial r_i} \left[\widehat{T}^{(2)} \right]^{-1}, \quad (10)$$

we get:

$$\forall i = 1, \dots, N \quad f_i^{elec} = \frac{dE_0(r_i)}{dr_i} p_i^* + \frac{1}{2} \widehat{p}^* \cdot \frac{\partial T^{(2)}}{\partial r_i} \widehat{p}^*. \quad (11)$$

If we now define:

$$\begin{aligned} T^{(3)}(r_{ij}) &= T^{(3)}(r_i - r_j) = \frac{\partial T^{(2)}(r_i - r_j)}{\partial r_i} \\ &= -\frac{r_i - r_j}{(4\pi\epsilon_0)^{1/2} r_{ij}^5} \left(6 \operatorname{erf}\left(\frac{r_{ij}}{a_{ij}}\right) - \frac{4}{\sqrt{\pi}} \left(3 \frac{r_{ij}}{a_{ij}} + 2 \frac{r_{ij}^3}{a_{ij}^3} + 2 \frac{r_{ij}^5}{a_{ij}^5} \right) \exp\left(-\frac{r_{ij}^2}{a_{ij}^2}\right) \right), \end{aligned} \quad (12)$$

one can show that:

$$\forall i, j, k = 1, \dots, N \quad \frac{\partial \left[\widehat{T}^{(2)} \right]_{j,k}}{\partial r_i} = T_{i,k}^{(3)} \delta_{i,j} - T_{j,i}^{(3)} \delta_{i,k}. \quad (13)$$

Using this result and the antisymmetry of $T^{(3)}$ with respect to the interchange of the two positions, the forces can now be written as:

$$\forall i = 1, \dots, N \quad f_i^{elec} = p_i^* \left(\frac{dE_0(r_i)}{dr_i} + \sum_{j=1}^N T_{ij}^{(3)} p_j^* \right), \quad (14)$$

We note that this result would simply be $f_i^{elec} = p_i^* dE_i/dr_i$ with $E_i = E_0(r_i) + \sum_{j=1}^N T_{ij}^{(2)} p_j^*$ the total electric field at r_i , if the p_j^* would not be functions of r_i , which they are, due to (6).

From Eqs. (9) and (14), we can see that the computation of the p_j^* and thus the inverse of the $N \times N$ system in (9) ($3N \times 3N$ in 3D) is the limiting step during the calculation of the electrostatic forces with this GDM model. As the inverse of this equation occurs for each iteration during the energy minimization process, practical use of it [39,40] was limited to carbon nanotubes with a number of atoms of the order of 5000. This is still far from what would be needed for realistic nanomaterials with sizes exceeding 10 nm in which nanoscale surface effects still lead to unexpected mechanical properties as compared to bulk materials [26].

4. Finite element equilibrium equations from total electromechanical potential energy

To significantly alleviate the computational expense incurred in a fully atomistic calculation of the electrostatic forces using the GDM, we propose an alternative approach in the present work, whereby we will obtain an FEM solution to minimizing the total energy U^{total} in (1). In essence, we will transform the problem of minimizing U^{total} from one that must be done for each and every atom in the system, to one in which the mechanical energy U^{mech} and electrostatic energy U^{elec} are evaluated only at FEM integration points. Furthermore, we will demonstrate below that (in 1D) the calculation of the bulk electrostatic stress does not require the inverse of an $N \times N$ system, while the calculation of the surface electrostatic stress requires the inverse of an $N_{surf} \times N_{surf}$ system only, where N_{surf} is on the order of 10 for sufficient accuracy as compared to benchmark fully atomistic calculations.

We accomplish this by applying the standard FEM displacement approximation to (1); doing so leads to FEM equilibrium equations which naturally reflect the self-consistent competition between mechanical and electrostatic forces. The details regarding the transition from the mechanical potential energy in (1) while delineating the bulk and surface energies to the FEM equilibrium equations is given in detail by Park et al. [46]; we note that the electrostatic potential energy including surface effects in (1) can be treated similarly. The final electromechanical FEM equilibrium equations that we implement and solve numerically are:

$$\begin{aligned} \frac{\partial U^{total}}{\partial \mathbf{u}_l} &= \int_{\Omega_0^{bulk}} \mathbf{B}^T \mathbf{P}^{mech} d\Omega + \int_{\Gamma_0} \mathbf{B}^T \widetilde{\mathbf{P}}^{mech} d\Gamma - \int_{\Gamma_0} N_l \mathbf{T} d\Gamma \\ &\quad + \int_{\Omega_0^{bulk}} \mathbf{B}^T \mathbf{P}^{elec} d\Omega + \int_{\Gamma_0} \mathbf{B}^T \widetilde{\mathbf{P}}^{elec} d\Gamma, \end{aligned} \quad (15)$$

where N_l are the FEM shape functions, $\mathbf{B}^T = \left(\frac{\partial N_l}{\partial \mathbf{x}} \right)^T$, \mathbf{T} are externally applied tractions, \mathbf{P}^{mech} is the bulk mechanical first Piola–Kirchhoff stress, \mathbf{P}^{elec} is the bulk electrostatic first Piola–Kirchhoff stress, $\widetilde{\mathbf{P}}^{mech}$ is the surface mechanical first Piola–Kirchhoff stress, and $\widetilde{\mathbf{P}}^{elec}$ is the surface electrostatic first Piola–Kirchhoff stress. Thus, the boundary value problem in (15) can be stated as: given an applied electric field \mathbf{E}_0 that is considered to be homogeneous in a given finite element and the applied external mechanical forces, find the atomic bond lengths r_{ij} that minimize the total electromechanical potential energy.

Because Park and co-authors have previously discussed how to obtain the bulk and surface mechanical stresses using the surface Cauchy–Born model [46], we will not cover that in this work, and will focus only on what is new, i.e. calculation of the bulk and surface electrostatic stresses. Furthermore, the method of evaluating both the bulk and surface integrals for the electrostatic stresses are identical to how the bulk and surface integrals are evaluated for the mechanical stresses; details are again given in Park et al. [46].

The FEM governing equations in (15) are novel and important because they demonstrate that: (1) a coupled electromechanical analysis of surface-dominated nanomaterials is possible solving only one governing equation, which fully accounts for the external electric field induced polarization-strain coupling between mechanical and electrostatic forces, including surface effects, and which obtains the required mathematical relationships for both the mechanical and electrostatic fields directly from underlying atomistic principles. (2) By changing the problem formulation from one that is computationally intractable, i.e. fully atomistic and involving millions of degrees of freedom, to one that is tractable, i.e. based on well-established FEM techniques with a significantly reduced number of degrees of freedom, we will achieve significant computational savings, as the FEM element size is typically 100–1000 times larger than the atomic spacing [47]. (3) The coupled electromechanical FEM governing equations are cast naturally in a total Lagrangian formulation, which ensures that no remeshing of the domain is required. (4) Because the FEM governing equation in (15) eliminates the need for any atomistic equations of motion, we will avoid both the time step and time scale issues that arise when using atomistic simulation techniques, though this implies that the externally applied electric field is constrained to be homogeneous within each finite element. We note that because the GDM approach, and specifically the electrostatic potential energy is, similar to mechanical interatomic potentials, dependent only on the distance r_{ij} between two atoms i and j , there is no issue applying the GDM approach to dynamic, or finite temperature problems so long as an appropriate parameterization of the atomic polarizabilities is available.

We now discuss how, using multiscale Cauchy–Born-based techniques, the bulk and surface mechanical and electrostatic stresses that are needed to solve (15) can be calculated in an efficient and accurate manner.

5. Bulk electrostatic Piola–Kirchhoff stress

5.1. Cauchy–Born kinematics

After having derived the expression for the electrostatic potential energy in (8), we utilize Cauchy–Born principles to first convert the electrostatic potential energy into an electrostatic energy

density, which we can then differentiate to obtain the electrostatic Piola–Kirchhoff stresses.

The Cauchy–Born model [46,82–84] has been utilized in recent years as a multiscale, hyperelastic material model that originates from a given interatomic potential energy function. The multiscale link between atomistics and continua is achieved by normalizing the interatomic potential by a representative volume and enforcing that the bond lengths between atoms r_{ij} are constrained to deform via the local value of the continuum deformation gradient \mathbf{F} or stretch tensor \mathbf{C} . In doing so, continuum stress and stiffness, which are needed for nonlinear FEM simulations, can be directly obtained by taking one and two derivatives, respectively, of the strain energy with respect to the continuum deformation measure. Because of the fact that continuum stress and stiffness can be derived directly from an atomistic interatomic potential, the Cauchy–Born model is regarded as a hierarchical multiscale constitutive model. However, it should be noted that while the Cauchy–Born hypothesis does lead to a multiscale link between atomistics and continua, it does also place a key restriction upon the deformation of the underlying crystal. Specifically, it enforces a locally homogeneous deformation assumption upon the underlying crystal by defining the deformed bond length $\mathbf{r} = \mathbf{F}\mathbf{r}_0$ between two atoms to be a function of the deformation gradient or stretch tensor at the corresponding finite element integration point.

To briefly overview Cauchy–Born kinematics, we note that in Green elastic theory, stress is derived by differentiating the material strain energy density function. In order to satisfy material frame indifference, the strain energy density must be expressed as a function of the right stretch tensor \mathbf{C} :

$$W(\mathbf{F}) = \Phi(\mathbf{C}), \quad (16)$$

where

$$\mathbf{C} = \mathbf{F}^T \mathbf{F}, \quad (17)$$

and \mathbf{F} is the deformation gradient. From the strain energy density, one can obtain the first (\mathbf{P}) and second (\mathbf{S}) Piola–Kirchhoff stresses as:

$$\mathbf{P} = \frac{\partial W(\mathbf{F})}{\partial \mathbf{F}^T} \quad \text{and} \quad \mathbf{S} = 2 \frac{\partial \Phi(\mathbf{C})}{\partial \mathbf{C}}, \quad (18)$$

where the Piola–Kirchhoff stresses are related by

$$\mathbf{P} = \mathbf{S}\mathbf{F}^T. \quad (19)$$

In the previous Cauchy–Born literature [46,82,83], the strain energy density was assumed to be a mechanical energy density which was obtained from an underlying atomistic interatomic potential, for example an embedded atom (EAM) potential for FCC metals [47,82], Brenner potentials for carbon [83,85], or Tersoff potentials for silicon [48,86].

In contrast to previous research that has utilized the Cauchy–Born hypothesis for mechanical problems, we utilize it here to obtain the electrostatic Piola–Kirchhoff stresses. To do so, we first consider the 1D bulk case, which can be interpreted as consideration of an infinite bulk chain of atoms in which all atoms have the same bonding environment, such that surface effects are not considered; we note that this is standard for Cauchy–Born approximations and that it is the reason why the surface Cauchy–Born model of Park et al. [46–48] was developed to account for the fact that the standard Cauchy–Born mechanical model does not admit surface effects.

Therefore, within this 1D electrostatic bulk idealization, all atoms have the same dipole moment p , and thus we can derive the electrostatic energy density by normalizing (2) by the equilibrium atomic lattice spacing r_0 , and by enforcing the Cauchy–Born hypothesis upon the deformed atomic lattice spacing $r = r_0 \sqrt{\mathbf{C}}$ to give:

$$\Phi^{elec}(\mathbf{C}) = \frac{1}{r_0} \left\{ -\frac{1}{2} \sum_{n=-\infty}^{\infty} (p_0 T^{(2)}(\mathbf{C}) p_n) - p_0 E_0 \right\}, \quad (20)$$

where for all n , $p_n = p_0 = p^*$ at electrostatic equilibrium for an infinite, periodic bulk system of identical atoms. Therefore, the electrostatic equilibrium condition, i.e. $\frac{d\Phi^{elec}}{dp}(p^*) = 0$ reduces to:

$$-p^* \sum_{n=-\infty}^{\infty} T^{(2)}(nr_0 \sqrt{\mathbf{C}}) - E_0 = 0. \quad (21)$$

Therefore the bulk dipoles p^* take the value:

$$p^*(\mathbf{C}) = -E_0 / \sum_{n=-\infty}^{\infty} T^{(2)}(nr_0 \sqrt{\mathbf{C}}), \quad (22)$$

and the electrostatic energy density can then be written using (20) as:

$$\Phi^{elec}(\mathbf{C}) = E_0^2 / \left(2r_0 \sum_{n=-\infty}^{\infty} T^{(2)}(nr_0 \sqrt{\mathbf{C}}) \right). \quad (23)$$

From (23), we can obtain the bulk electrostatic second Piola–Kirchhoff stress as:

$$\begin{aligned} S^{elec}(\mathbf{C}) &= 2 \frac{d\Phi^{elec}}{d\mathbf{C}} \\ &= -\frac{E_0^2}{r_0} \frac{d}{d\mathbf{C}} \left(\sum_{n=-\infty}^{\infty} T^{(2)}(nr_0 \sqrt{\mathbf{C}}) \right) / \left(\sum_{n=-\infty}^{\infty} T^{(2)}(nr_0 \sqrt{\mathbf{C}}) \right)^2, \end{aligned} \quad (24)$$

which using definition (12) can be rewritten as:

$$\begin{aligned} S^{elec}(\mathbf{C}) &= -\frac{E_0^2}{r_0} \sum_{n=-\infty}^{\infty} \left(T^{(3)}(nr_0 \sqrt{\mathbf{C}}) \frac{nr_0}{2\sqrt{\mathbf{C}}} \right) / \left(\sum_{n=-\infty}^{\infty} T^{(2)}(nr(\mathbf{C})) \right)^2, \\ &= -\frac{E_0^2 r_0}{2r} \sum_{n=-\infty}^{\infty} \left(T^{(3)}(nr(\mathbf{C})) n \right) / \left(\sum_{n=-\infty}^{\infty} T^{(2)}(nr(\mathbf{C})) \right)^2, \\ &= -\frac{E_0^2 r_0}{r} \sum_{n=1}^{\infty} \left(T^{(3)}(nr(\mathbf{C})) n \right) / \left(\sum_{n=-\infty}^{\infty} T^{(2)}(nr(\mathbf{C})) \right)^2. \end{aligned} \quad (25)$$

Finally, the bulk electrostatic first Piola–Kirchhoff stress can be obtained by using the standard continuum mechanics relationship in (19), while noting that in 1D, $F = F^T = \sqrt{\mathbf{C}} = r/r_0$ and

$$\begin{aligned} P^{elec} &= -F \frac{E_0^2 r_0}{2r} \sum_{n=-\infty}^{\infty} \left(T^{(3)}(nr(F)) n \right) / \left(\sum_{n=-\infty}^{\infty} T^{(2)}(nr(F)) \right)^2, \\ &= -E_0^2 \sum_{n=1}^{\infty} \left(n T^{(3)}(nr(F)) \right) / \left(\sum_{n=-\infty}^{\infty} T^{(2)}(nr(F)) \right)^2. \end{aligned} \quad (26)$$

5.2. Comparison of bulk electrostatic stress to MD electrostatic force

It is important to compare here the computational advantages gained in the expression for the bulk electrostatic stress in (25) in comparison to the electrostatic forces (14). First, we note that no matrix inverse is required to compute the bulk electrostatic stress in (25). Instead, only the calculation of discrete sums for the dipole interaction tensors $T^{(2)}$ and $T^{(3)}$ are required, where we have found that extending both summations to about $n = 20$ is sufficient to obtain a converged response. These sums of interaction tensors will be called periodized interaction tensors. We note that for 3D problems, the inverse of a $3N_{per} \times 3N_{per}$ system will be needed at each FEM integration point, where N_{per} is the number of atoms in the 3D lattice unit cell (i.e. 1 for an FCC crystal), provided periodized 3D interaction tensors are used.

Second, we note that the computational expense in calculating the electrostatic stress in (25) is reduced dramatically as compared to the computation of the forces in the full system of N atoms not only because the system size is significantly smaller, but also because the electrostatic stress is calculated only at FEM integration points, such that it is evaluated at far fewer points in the domain than the electrostatic force, which is evaluated (at significantly greater computational expense) for every atom in the domain.

6. Surface electrostatic stress

The final aspect to the coupled electromechanical formulation is to calculate the surface electrostatic stress; we now present the derivation in 1D. In nanomechanics, surface effects play a significant role in causing nanostructures to exhibit non-bulk mechanical properties as compared to the corresponding bulk material [26]. The surface effects arise because atoms at or near the surfaces of the material have fewer bonding neighbors than do atoms in the bulk, which alters their elastic properties as compared to the bulk atoms.

Similar effects occur in electrostatics; specifically, because atoms at the surface have fewer bonding neighbors, their effective dipolar polarizability tensor α_i is different, which leads to atoms at or near the surface polarizing differently and thus having a different dipole moment in response to an applied electric field as compared to bulk atoms [35–38].

In the present work, we assume that, for each surface finite element integration point, we have n_{surf} surface atoms with indices $i \leq 0$, while atoms $i > 0$ are bulk atoms, i.e. they all have the same dipole moment p^* , as computed using (22). We assume that the atoms initially have positions $x_i = ir_0$ before the homogeneous deformation due to the deformation gradient F and that the external electrostatic field E_0 is also homogeneous in the small volume corresponding to the integration point. Then, the system of equations to solve for the surface dipoles p_j^s is based upon a modification of the bulk dipole solution in (22) to give, for all $i \leq 0$:

$$\sum_{j=-n_{surf}+1}^0 T^{(2)}((i-j)r_0F)p_j^s = -E_0 - \sum_{n=1}^{\infty} T^{(2)}((i-n)r_0F)p^*. \quad (27)$$

The surface energy density (energy per unit surface area) is then written as:

$$\begin{aligned} \tilde{\phi}^{elec}(F) &= \left(-\frac{1}{2} \sum_{i=-n_{surf}+1}^0 \sum_{m=-n_{surf}+1}^{\infty} p_i^s T^{(2)}((i-m)Fr_0) p_m \right) \\ &\quad - \sum_{i=-n_{surf}+1}^0 p_i^s E_0 = -\frac{1}{2} \sum_{i=-n_{surf}+1}^0 p_i^s(F) E_0. \end{aligned} \quad (28)$$

Consequently, we define the surface electrostatic first Piola–Kirchhoff stress as:

$$\tilde{P}^{elec}(F) = \frac{d\tilde{\phi}^{elec}}{dF^T} = -\frac{E_0}{2} \sum_{i=-n_{surf}+1}^0 \frac{dp_i^s}{dF^T}, \quad (29)$$

where for all $i \leq 0$ by solving (27):

$$p_i^s = \sum_{j=-n_{surf}+1}^0 \left\{ \left[\widehat{T}^{(2)} \right]_{ij}^{-1} \left(-E_0 - \sum_{n=1}^{\infty} T^{(2)}((j-n)Fr_0)p^* \right) \right\}, \quad (30)$$

and thus the surface electrostatic first Piola–Kirchhoff stress is:

$$\begin{aligned} \tilde{P}^{elec}(F) &= -\frac{E_0}{2} \sum_{i=-n_{surf}+1}^0 \sum_{j=-n_{surf}+1}^0, \\ &\quad \frac{d}{dF} \left[\left[\widehat{T}^{(2)} \right]_{ij}^{-1} \left(-E_0 - \sum_{n=1}^{\infty} T^{(2)}((j-n)Fr_0)p^* \right) \right]. \end{aligned} \quad (31)$$

To evaluate the derivative in (31), we use an approach similar to what was done for the computation of the forces in Section 3.2. Using Eq. (12), we first get:

$$\frac{dT_{ij}^{(2)}}{dF} = \frac{dT^{(2)}((i-j)Fr_0)}{dF} = (i-j)r_0T^{(3)}((i-j)Fr_0). \quad (32)$$

Now, using this and the fact that:

$$\widehat{T}^{(2)} \left[\widehat{T}^{(2)} \right]^{-1} = \mathbf{I} \Rightarrow \frac{d \left[\widehat{T}^{(2)} \right]^{-1}}{dF} = - \left[\widehat{T}^{(2)} \right]^{-1} \frac{d \widehat{T}^{(2)}}{dF} \left[\widehat{T}^{(2)} \right]^{-1}, \quad (33)$$

we get:

$$\frac{d \left[\widehat{T}^{(2)} \right]^{-1}}{dF} = -r_0 \left[\widehat{T}^{(2)} \right]^{-1} \left[(i-j)T_{ij}^{(3)} \right] \left[\widehat{T}^{(2)} \right]^{-1}. \quad (34)$$

Furthermore, since $p^* = -E_0 / \sum_{n=-\infty}^{\infty} T^{(2)}(nFr_0)$ we have:

$$\begin{aligned} \frac{d \left(-E_0 - \sum_{n=1}^{\infty} T^{(2)}((j-n)Fr_0)p^* \right)}{dF} &= E_0 \frac{d}{dF} \left[\frac{\sum_{n=1}^{\infty} T^{(2)}((j-n)Fr_0)}{\sum_{n=-\infty}^{\infty} T^{(2)}(nFr_0)} \right] \\ &= E_0 r_0 \left[\frac{\sum_{n=1}^{\infty} (j-n)T^{(3)}((j-n)Fr_0)}{\sum_{n=-\infty}^{\infty} T^{(2)}(nFr_0)} \right] \\ &\quad - \left[\frac{\sum_{n=1}^{\infty} T^{(2)}((j-n)Fr_0) \sum_{n=-\infty}^{\infty} nT^{(3)}(nFr_0)}{\left(\sum_{n=-\infty}^{\infty} T^{(2)}(nFr_0) \right)^2} \right]. \end{aligned} \quad (35)$$

Putting (34) and (35) into (31) and using (27), the surface electrostatic stress can be written as:

$$\begin{aligned} \tilde{P}^{elec}(F) &= \frac{E_0 r_0}{2} \sum_{i=-n_{surf}+1}^0 \sum_{k=-n_{surf}+1}^0 \sum_{l=-n_{surf}+1}^0 \left[\widehat{T}^{(2)} \right]_{i,k}^{-1} (k-l)T^{(3)}((k-l)Fr_0)p_i^s \\ &\quad + \frac{E_0 r_0 p^*}{2} \sum_{i=-n_{surf}+1}^0 \sum_{j=-n_{surf}+1}^0 \left[\widehat{T}^{(2)} \right]_{ij}^{-1} \sum_{n=1}^{\infty} (j-n)T^{(3)}((j-n)r_0F) \\ &\quad + \frac{r_0 (p^*)^2}{2} \left(\sum_{n=-\infty}^{\infty} nT^{(3)}(nFr_0) \right) \sum_{i=-n_{surf}+1}^0 \sum_{j=-n_{surf}+1}^0 \left\{ \left[\widehat{T}^{(2)} \right]_{ij}^{-1} \right. \\ &\quad \left. \sum_{n=1}^{\infty} T^{(2)}((j-n)r_0F) \right\}. \end{aligned} \quad (36)$$

There are several relevant points to be discussed before moving onto the numerical examples. First, it is seen in both (36) and (30) that the inverse of the dipole–dipole interaction tensor $T^{(2)}$ is required to calculate both the surface dipoles and thus the electrostatic stress, where the size of the tensor is related to the number of surface atoms (n_{surf}) that are considered. We will show in the numerical examples that in 1D, a value of $n_{surf} = 10$ or 15 gives results with accuracy that is comparable to the fully atomistic calculations. However, in 3D, limiting the value of n_{surf} will clearly be critical in keeping the computational expense to be minimal; we plan to investigate techniques pioneered in truncating Ewald sums to finite distances [87,88] for this purpose in future research.

7. 1D Numerical examples

7.1. Verification of bulk electrostatic stress

We first validate the bulk electrostatic stress. To do so, we compare results obtained from applying an external electric field ranging between 0.025 and 0.5 V/Å to an infinite 1D chain of atoms, where the physical parameters for the GDM were taken to mimic the values for carbon nanotubes [45,39], i.e. the equilibrium lattice spacing $r_0 = 3 \text{ \AA}$, and the isotropic polarizability $\alpha = 5.5086 \text{ \AA}^3$, while the width of the distribution R can be found from Eq. (5) of Mayer [45] to be 1.13576 Å.

For the mechanical response, we utilized a standard Lennard-Jones 6–12 potential, which takes the form:

$$U_{LJ}(r_{ij}) = 4\epsilon \left(\left(\frac{\sigma}{r_{ij}} \right)^{12} - \left(\frac{\sigma}{r_{ij}} \right)^6 \right), \quad (37)$$

where the parameters for the LJ potential were $\sigma = 2.6727 \text{ \AA}$, and $\epsilon = 0.4096 \text{ eV}$; the choice of σ ensured that the equilibrium lattice spacing for the mechanical LJ potential was also 3 \AA . Finally, in the mechanical problem, each atom was assumed to interact only with its nearest neighbors.

The minimum energy configuration of the fully atomistic system was systematically obtained by varying the deformation gradient F between 0.96 and 1.04 while evaluating both the electrostatic potential energy in (8) and the mechanical potential energy in (37) for a single, representative bulk atom. The varying deformation gradient is used to deform the surrounding bulk atoms as to evaluate changes in both the electrostatic and mechanical potential energies. The electrostatic potential energy was calculated for a single bulk atom that was surrounded by 100 nearest neighbors on each side to represent a bulk, infinite crystal.

Similarly, the minimum energy configuration of the bulk Cauchy–Born (BCB)-based FEM model was obtained by evaluating the weak form in (15), while neglecting both the surface electrostatic and mechanical stresses for an arbitrary domain size with a single linear finite element. Note that because all representative bulk atoms are identical, a single element is sufficient to capture the deformation due to the externally applied electric field.

The results are summarized in Table 1, while the mechanical, electrostatic and total potential energies are shown for the $E_0 = 0.25 \text{ V/\AA}$ fully atomistic case in Fig. 1. As can be seen in Table 1, the amount of strain that is incurred by subjecting an infinite, bulk 1D chain of atoms increases with an increase in the electric field intensity. Furthermore, the BCB results compare extremely well to the benchmark MD simulations for the wide range of applied electric field values that we have considered that result in both very small ($E_0 = 0.025 \text{ V/\AA}$), and finite ($E_0 = 0.5 \text{ V/\AA}$) strains. It is also interesting to point out that while the error remains essentially constant with an increase in electric field strength, Table 1 shows that the strain is proportional to E_0^2 , which is called the electrostriction effect. This is expected because the bulk first Piola–Kirchhoff stress is also proportional to E_0^2 , as shown in Eq. (25).

The good agreement between MD and BCB simulations enables us to move forward with confidence to including surface effects through the surface electrostatic stress, which we discuss in the next section.

7.2. Verification of surface electrostatic stress

We now discuss numerical validation of the proposed coupled electromechanical SCB model as compared to benchmark fully atomistic calculations. To do so, we considered 1D atomic chains of various length with fixed/free boundary conditions, as illustrated in Fig. 2. The externally applied electric field E_0 was applied in the positive x -direction parallel to the chain of atoms. We took two values of the external electric field, $E_0 = 0.1 \text{ V/\AA}$, and to test

Table 1
Comparison of strain (in percent) for bulk, infinite 1D chain of atoms due to externally applied electric field E_0 .

E_0 (V/\AA)	MD strain (%)	BCB strain (%)	Error in strain (%)
0.025	-0.00659	-0.00656	0.54
0.05	-0.0265	-0.02624	0.96
0.1	-0.1056	-0.1048	0.79
0.25	-0.6495	-0.6463	0.48
0.5	-2.4617	-2.4738	0.49

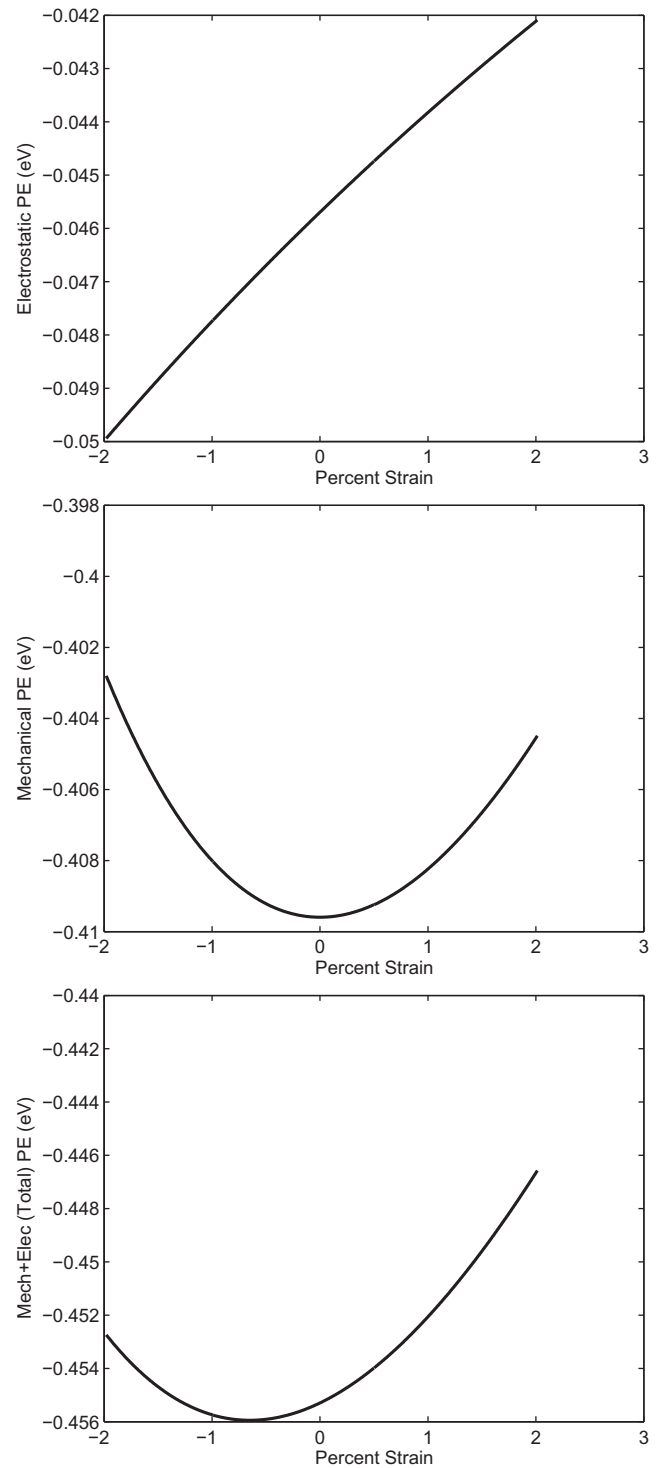


Fig. 1. Example of mechanical, electrostatic and total potential energy for an infinite 1D chain of atoms subject to an externally applied electric field of $E_0 = 0.25 \text{ V/\AA}$.

the nonlinear, finite deformation response, $E_0 = 0.5 \text{ V/\AA}$. A summary of all simulations and comparisons to fully atomistic calculations is shown in Table 2.

We first considered a 1D chain of 51 atoms subject to an applied electric field of 0.1 V/\AA , which was equivalently modeled using the SCB approach using 3 linear finite elements. While the bulk and surface electrostatic stresses were calculated using the formulation presented in this manuscript, the bulk and surface mechanical

stresses were calculated using the previously developed SCB model; details on the SCB implementation for a LJ potential in 1D was presented by Park et al. [46].

The numerical results are shown in Fig. 3, where the MD results, the SCB results for various values of n_{surf} , and BCB results are shown. First, we notice that the displacement field of the 1D chain is negative, or compressive, though the electric field is applied in the positive x -direction. Physically, this occurs because neighboring dipoles attract each other when they are aligned in the direction of the applied electric field.

There are other interesting effects that can be observed in comparing the finite chain (MD) and infinite chain (BCB) results. Specifically, it can be seen that the slope of the compressive displacement field becomes smaller near the free surfaces, and thus the deformation of the finite chain is smaller than the infinite chain by more than 9%, which demonstrates the importance of accounting for the electromechanical surface effects. This occurs due to the reduced polarization that occurs at the free surfaces.

It is also worth emphasizing here that for this, and all comparisons between the MD, BCB and SCB results, the key value that must be validated is that the SCB and MD results agree well, which is indeed demonstrated in Fig. 3. Because the problem is 1D, and because the mechanical potential energy is modeled using the LJ potential, which does not represent the behavior of any real material, the actual value of the surface effect is irrelevant; instead, the important point is that the MD and SCB results agree well, since they are both based upon the same mechanical and electrostatic potential energies.

For the SCB/MD comparison, we took the number of elements to be fixed at 3, and instead varied between 5 and 15 the number of surface atoms (n_{surf} in (26), (28)–(36)) for which we computed dipoles. The results demonstrate convergence of the SCB solution to the full MD solution as the number of surface atoms n_{surf} is increased, in accordance with expectation. Overall, while the SCB solution captures the surface effects, it is clear in Fig. 3 that the accuracy of the solution, particularly near the free end of the chain, increases with increasing n_{surf} . The error in the free end displacement decreases from 3.9% when $n_{surf} = 5$ to 1.3% when $n_{surf} = 10$ to 0.5% when $n_{surf} = 15$. We also note that quantifying the error introduced in truncating the surface dipoles is critical because the inverse of an $n_{surf} \times n_{surf}$ matrix is required at the surface to obtain the surface stress; thus it is important to have a small number of atoms n_{surf} to keep computational efficiency as compared to the benchmark MD solution, particularly as future extensions to 3D are made.

We also tested the accuracy of the SCB model for a larger system, that of a 101 atom 1D chain with the same fixed/free bound-

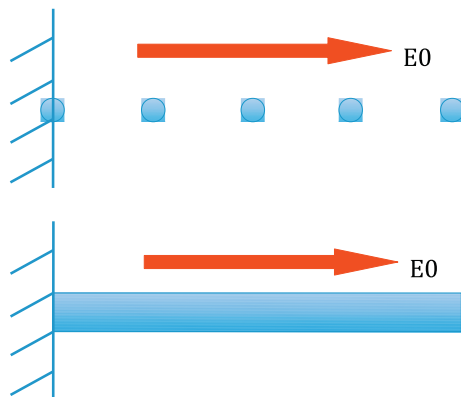


Fig. 2. Schematic of 1D chain of atoms subject to externally applied electric field E_0 . Top figure indicates discrete, atomistic model while bottom figure indicates the equivalent continuum model.

ary conditions, where the results for the BCB, MD and SCB simulations are given in Fig. 4. There are noticeable differences between the MD, BCB and SCB results as compared to the 51 atom case in Fig. 3. Most notably, the error between the BCB and MD solutions is only about 4.4% for the free end displacement, which is about half that of the 51 atom case. This is anticipated because the surface effects become less significant for the 101 atom chain.

The error introduced using the SCB model for the 101 atom case was also significantly smaller than for the 51 atom case. Specifically, the error in the end atom displacement was 1.86% when $n_{surf} = 5$, 0.6% when $n_{surf} = 10$, and 0.23% when $n_{surf} = 15$. The error is smaller as compared to the 51 atom case because the surface electrostatic effects are minimized due to the fact that more atoms are contained within the bulk of the material as compared to the 51 atom case. We also quantified the surface effect by calculating the dipole moments using fully atomistic simulations on a very long 1D chain. We found that the values for the dipole moment did not approach 99% of the bulk dipole moment until about 14 atoms into the bulk from the free surface. Thus, for the 51 atom chain, more than half of the atoms can be considered to have a non-bulk dipole moment, thus leading to the much stronger surface effects and difference as compared to the BCB value than was found for the 101 atom chain.

To further investigate both the larger surface effects and the finite deformation induced by the electric field, we re-considered the 51-atom case with a larger externally applied electric field of $E_0 = 0.5 \text{ V/\AA}$, with the results shown in Fig. 5. We see that the compressive displacement is significantly larger with the enhanced electric field, i.e. the compressive displacement of the free end of the 1D chain is nearly 4 \AA , for a strain of nearly 2.5%. Despite this, the SCB results show similar trends as for the previous 51 atom case subject to smaller electric field in that with an increase in n_{surf} , the SCB solution converges to the fully atomistic result despite the highly nonlinear deformation. Specifically, the error between the SCB and MD solutions is about 4.5% when $n_{surf} = 5$, but decreases to 0.6% when $n_{surf} = 15$. Furthermore, the effect of elastic nonlinearity can be observed by comparing the free end displacement for the 51 atom chain subject to the fields of 0.5 and 0.1 V/\AA as seen in Table 2. Specifically, the free end displacement for the 0.5 V/\AA case is only 23.5 times the 0.1 V/\AA case, which suggests as expected that the ideal linear electrostriction relationship, which is proportional to E_0^2 , breaks down at larger strains.

8. Conclusions and future research

We have presented in 1D a novel multiscale, finite deformation finite element approach to solving coupled electromechanical boundary value problems in which surface-dominated nanostructures are subject to externally applied electric fields. The key step was to create a multiscale total electromechanical potential energy based upon previous, purely atomistic electromechanical total energies [39,40]. In doing so, and in utilizing standard Cauchy–Born kinematics, we were able to derive a new coupled electromechanical variational form that has significant advantages as compared to previous electromechanical coupling approaches. Specifically, the coupled electromechanical response is obtained solving only one governing equation using the finite element method, which was made possible through derivation of new analytic formulas for the electrostatic forces, as well as both the bulk and surface electrostatic Piola–Kirchhoff stresses. In doing so, previous issues including the solution of the equations of both the mechanical and electrostatic domains are avoided, as are issues with deriving the coupling matrix between mechanical and electrostatic domains, while issues related to remeshing either the electrostatic and mechanical domains are also eliminated. The

Table 2

Comparison of percent error in free end displacement for 51 and 101 atom 1D chains for various applied electric fields between SCB for various values of n_{surf} and fully atomistic calculations. All displacements are in Å, values in parenthesis are the percent error as compared to the benchmark MD solution.

Atoms	E_0 (V/Å)	MD	SCB $n_{surf} = 5$	SCB $n_{surf} = 10$	SCB $n_{surf} = 15$
51	0.1	-0.1439	-0.1496 (3.9%)	-0.1458 (1.3%)	-0.1447 (0.5%)
51	0.5	-3.376	-3.528 (4.5%)	-3.4281 (1.54%)	-3.397 (0.6%)
101	0.1	-0.303	-0.308 (1.86%)	-0.3044 (0.6%)	-0.303 (0.23%)

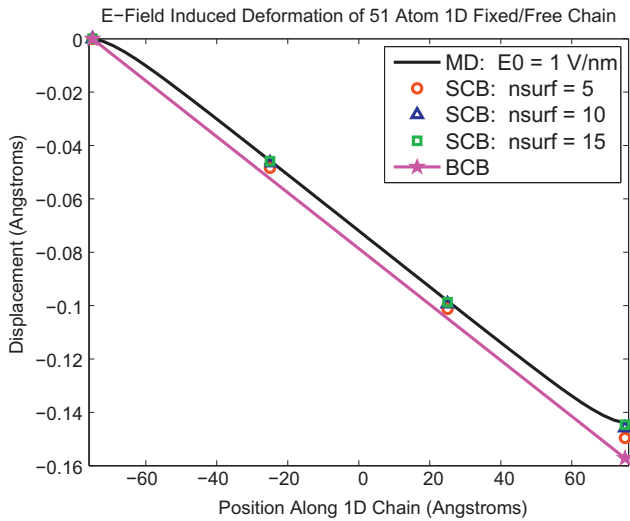


Fig. 3. Comparison between full MD and SCB results for a 51 atom 1D chain subject to externally applied electric field of $E_0 = 0.1$ V/Å. BCB result also shown to indicate how surface effect impact the deformation of 1D chain to an electric field.

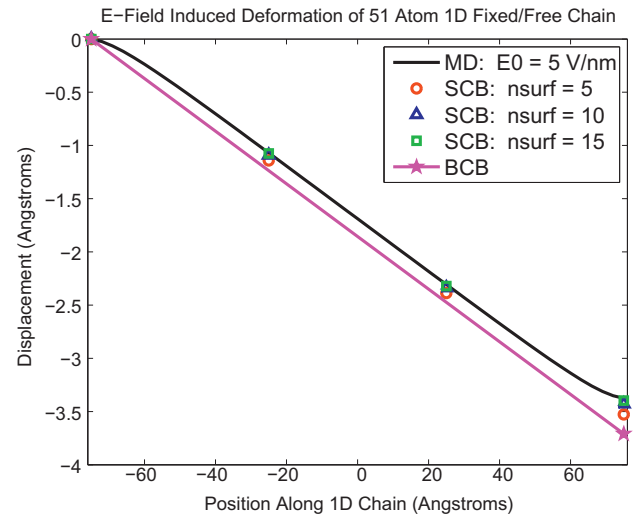


Fig. 5. Comparison between full MD and SCB results for a 51 atom 1D chain subject to externally applied electric field of $E_0 = 0.5$ V/Å. BCB result also shown to indicate how surface effect impact the deformation of 1D chain to an electric field.

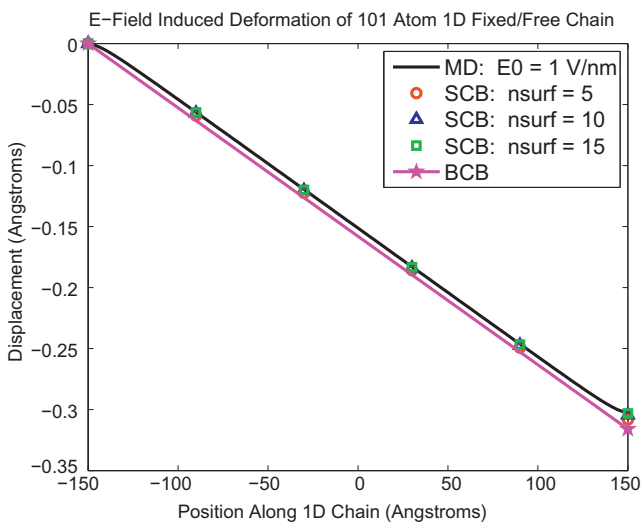


Fig. 4. Comparison between full MD and SCB results for a 101 atom 1D chain subject to externally applied electric field of $E_0 = 0.1$ V/Å. BCB result also shown to indicate how surface effect impact the deformation of 1D chain to an electric field.

method was validated and shown to be accurate in comparison with fully atomistic electromechanical calculations in one dimension.

While the approach was based upon finite deformation Cauchy–Born kinematics, the utilization of the Cauchy–Born hypothesis indicates that defect nucleation cannot be captured without modifications to the method. Indeed, defect nucleation can be captured by adopting the quasicontinuum technique [82], whereby the finite element mesh is meshed down to the atomic scale at or near

regions where defect nucleation may occur. However, the Cauchy–Born kinematics are valid for large, nonlinear elastic deformations, which are known not only to occur in nanowires [32], but to have a significant effect on their mechanical behavior and properties [34].

The key challenge in extending this approach to three-dimensions lies solely with the electrostatic domain, as surface Cauchy–Born models for the mechanical domain have already been developed for both FCC metals [47], and semiconductors such as silicon [48]. Specifically, the challenge is first to generalize the analytic formulas for the electrostatic forces and Piola–Kirchhoff stresses to the 3D case, then to keep to a minimal size the number of surface atoms n_{surf} that are needed to calculate surface dipoles and thus the surface electrostatic stress because the size of the matrix that is needed to be inverted to obtain the surface electrostatic stress is directly proportional to n_{surf} . Techniques for accomplishing this are currently under evaluation.

Acknowledgments

Harold S. Park gratefully acknowledges the support of NSF Grant CMMI-0856261 for this research, and valuable discussions with Patrick A. Klein.

References

- [1] W. Guo, Y. Guo, Giant axial electrostrictive deformation in carbon nanotubes, *Phys. Rev. Lett.* 91 (2003) 115501.
- [2] K. El-Hami, K. Matsushige, Electrostriction in single-walled carbon nanotubes, *Ultramicroscopy* 105 (2005) 143–147.
- [3] H.J. Mamin, D. Rugar, Sub-atto-newton force detection at millikelvin temperatures, *Appl. Phys. Lett.* 79 (2001) 3358–3360.
- [4] M.D. LaHaye, O. Buu, B. Camarota, K.C. Schwab, Approaching the quantum limit of a nanomechanical resonator, *Science* 304 (2004) 74–77.
- [5] R.G. Knobel, A.N. Cleland, Nanometre-scale displacement sensing using a single electron transistor, *Nature* 424 (2003) 291–293.

- [6] K. Jensen, K. Kim, A. Zettl, An atomic-resolution nanomechanical mass sensor, *Nat. Nanotechnol.* 3 (2008) 533–537.
- [7] K.L. Ekinici, M.L. Roukes, Nanoelectromechanical systems, *Rev. Sci. Instrum.* 76 (2005) 061101.
- [8] Q.P. Unterreithmeier, E.M. Weig, J.P. Kotthaus, Universal transduction scheme for nanomechanical systems based on dielectric forces, *Nature* 458 (2009) 1001–1004.
- [9] Y. Zhang, A. Chang, J. Cao, Q. Wang, W. Kim, Y. Li, N. Morris, E. Yenilmez, J. Kong, H. Dai, Electric-field-directed growth of aligned single-walled carbon nanotubes, *Appl. Phys. Lett.* 79 (2001) 3155–3157.
- [10] C.Q. Chen, Y. Shi, Y.S. Zhang, J. Zhu, Y.J. Yan, Size dependence of the young's modulus of ZnO nanowires, *Phys. Rev. Lett.* 96 (2006) 075505.
- [11] P. Poncharal, Z.L. Wang, D. Ugarte, W.A. de Heer, Electrostatic deflections and electromechanical resonances of carbon nanotubes, *Science* 283 (1999) 1513–1516.
- [12] Y. Wei, C. Xie, K.A. Dean, B.F. Coll, Stability of carbon nanotubes under electric field studied by scanning electron microscopy, *Appl. Phys. Lett.* 79 (2001) 4527–4529.
- [13] Y. Guo, W. Guo, Mechanical and electrostatic properties of carbon nanotubes under tensile loading and electric field, *J. Phys. D: Appl. Phys.* 36 (2003) 805–811.
- [14] Z. Wang, L. Philippe, Deformation of doubly clamped single-walled carbon nanotubes in an electrostatic field, *Phys. Rev. Lett.* 102 (2009) 215501.
- [15] N.R. Aluru, J. White, An efficient numerical technique for electromechanical simulation of complicated microelectromechanical structures, *Sensor Actuator A* 58 (1997) 1–11.
- [16] S.D. Senturia, R.M. Harris, B.P. Johnson, S. Kim, K. Nabors, M.A. Shulman, J.K. White, A computer-aided design system for microelectromechanical systems (MEMCAD), *J. Microelectromech. Syst.* 1 (1992) 3–13.
- [17] F. Shi, P. Ramesh, S. Mukherjee, Dynamic analysis of micro-electro-mechanical systems, *Int. J. Numer. Methods Engrg.* 39 (1996) 4119–4139.
- [18] S.K. De, N.R. Aluru, Full-Lagrangian schemes for dynamic analysis of electrostatic MEMS, *J. Microelectromech. Syst.* 13 (2004) 737–758.
- [19] A. Soma, F.D. Bona, A. Gugliotta, E. Mola, Meshing approach in non-linear FEM analysis of microstructures under electrostatic loads, *Proc. SPIE* 4408 (2001) 216–225.
- [20] G. Li, N.R. Aluru, A Lagrangian approach for electrostatic analysis of deformable conductors, *J. Microelectromech. Syst.* 11 (2002) 245–254.
- [21] S. Telukunta, S. Mukherjee, Fully Lagrangian modeling of MEMS with thin plates, *J. Microelectromech. Syst.* 15 (2006) 795–810.
- [22] P.S. Sumant, N.R. Aluru, A.C. Cangellaris, A methodology for fast finite element modeling of electrostatically actuated MEMS, *Int. J. Numer. Methods Engrg.* 77 (2009) 1789–1808.
- [23] G.-H. Kim, K.C. Park, A continuum-based modeling of MEMS devices for estimating their resonant frequencies, *Comput. Methods Appl. Mech. Engrg.* 198 (2008) 234–244.
- [24] G.-H. Kim, Partitioned analysis of electromagnetic field problems by localized Lagrange multipliers, Technical report, Center for Aerospace Structures, University of Colorado at Boulder, 2006.
- [25] R.C. Cammarata, Surface and interface stress effects in thin films, *Prog. Surf. Sci.* 46 (1994) 1–38.
- [26] H.S. Park, W. Cai, H.D. Espinosa, H. Huang, Mechanics of crystalline nanowires, *MRS Bull.* 34 (2009) 178–183.
- [27] R. Agrawal, B. Peng, E. Gdoutos, H.D. Espinosa, Elasticity size effects in ZnO nanowires – a combined experimental–computational approach, *Nano Lett.* 8 (2008) 3668–3674.
- [28] S. Cuenot, C. Frétygny, S. Demoustier-Champagne, B. Nysten, Surface tension effect on the mechanical properties of nanomaterials measured by atomic force microscopy, *Phys. Rev. B* 69 (2004) 165410.
- [29] Y. Zhu, F. Xu, Q. Qin, W.Y. Fung, W. Lu, Mechanical properties of vapor–liquid–solid synthesized silicon nanowires, *Nano Lett.* 9 (2009) 3934–3939.
- [30] R.E. Miller, V.B. Shenoy, Size-dependent elastic properties of nanosized structural elements, *Nanotechnology* 11 (2000) 139–147.
- [31] L.G. Zhou, H. Huang, Are surfaces elastically softer or stiffer?, *Appl Phys. Lett.* 84 (2004) 1940–1942.
- [32] H. Liang, M. Upmanyu, H. Huang, Size-dependent elasticity of nanowires: nonlinear effects, *Phys. Rev. B* 71 (2005) 241403(R).
- [33] J. Diao, K. Gall, M.L. Dunn, Atomistic simulation of the structure and elastic properties of gold nanowires, *J. Mech. Phys. Solids* 52 (2004) 1935–1962.
- [34] H.S. Park, P.A. Klein, Surface stress effects on the resonant properties of metal nanowires: the importance of finite deformation kinematics and the impact of the residual surface stress, *J. Mech. Phys. Solids* 56 (2008) 3144–3166.
- [35] M. Guillaume, B. Champagne, D. Begue, C. Pouchan, Electrostatic interaction schemes for evaluating the polarizability of silicon clusters, *J. Chem. Phys.* 130 (2009) 134715.
- [36] A. Mayer, A.L. Gonzales, C.M. Aikens, G.C. Schatz, A charge-dipole interaction model for the frequency-dependent polarizability of silver clusters, *Nanotechnology* 20 (2009) 195204.
- [37] L.L. Jensen, L. Jensen, Electrostatic interaction model for the calculation of the polarizability of large noble metal nanostructures, *J. Phys. Chem. C* 112 (2008) 15697–15703.
- [38] L.L. Jensen, L. Jensen, Atomistic electrostatics model for optical properties of silver nanoclusters, *J. Phys. Chem. C* 113 (2009) 15182–15190.
- [39] Z. Wang, M. Devel, R. Langlet, B. Dulmet, Electrostatic deflections of cantilevered semiconducting single-walled carbon nanotubes, *Phys. Rev. B* 75 (2007) 205414.
- [40] Z. Wang, M. Devel, Electrostatic deflections of cantilevered metallic carbon nanotubes via charge-dipole model, *Phys. Rev. B* 76 (2007) 195434.
- [41] S.J. Stuart, A.B. Tutein, J.A. Harrison, A reactive potential for hydrocarbons with intermolecular interactions, *J. Chem. Phys.* 112 (2000) 6472–6486.
- [42] J. Mahanty, B.W. Ninham, *Dispersion Forces*, Academic Press, New York, 1976.
- [43] R. Langlet, M. Arab, F. Picaud, M. Devel, C. Girardet, Influence of molecular adsorption on the dielectric properties of a single wall carbon nanotube: a model sensor, *J. Comput. Phys.* 121 (2004) 9655–9665.
- [44] A. Mayer, P. Lambin, R. Langlet, Charge-dipole model to compute the polarization of fullerenes, *Appl. Phys. Lett.* 89 (2006) 063117.
- [45] A. Mayer, Formulation in terms of normalized propagators of a charge-dipole model enabling the calculation of the polarization properties of fullerenes and carbon nanotubes, *Phys. Rev. B* 75 (2007) 045407.
- [46] H.S. Park, P.A. Klein, G.J. Wagner, A surface Cauchy–Born model for nanoscale materials, *Int. J. Numer. Methods Engrg.* 68 (2006) 1072–1095.
- [47] H.S. Park, P.A. Klein, Surface Cauchy–Born analysis of surface stress effects on metallic nanowires, *Phys. Rev. B* 75 (2007) 085408.
- [48] H.S. Park, P.A. Klein, A surface Cauchy–Born model for silicon nanostructures, *Comput. Methods Appl. Mech. Engrg.* 197 (2008) 3249–3260.
- [49] G. Yun, H.S. Park, Surface stress effects on the bending properties of fcc metal nanowires, *Phys. Rev. B* 79 (2009) 195421.
- [50] H.S. Park, Surface stress effects on the resonant properties of silicon nanowires, *J. Appl. Phys.* 103 (2008) 123504.
- [51] H.S. Park, Quantifying the size-dependent effect of the residual surface stress on the resonant frequencies of silicon nanowires if finite deformation kinematics are considered, *Nanotechnology* 20 (2009) 115701.
- [52] J.M. Haile, *Molecular Dynamics Simulations*, Wiley and Sons, 1992.
- [53] A. Leach, *Molecular Modelling: Principles and Applications*, Pearson Education Limited, 2001.
- [54] L. Silberstein, Dispersion and the size of molecules of hydrogen, oxygen, and nitrogen, *Philos. Mag.* 33 (1917) 215–222.
- [55] L. Silberstein, Molecular refractivity and atomic interaction, *Philos. Mag.* 33 (1917) 92–128.
- [56] L. Silberstein, Molecular refractivity and atomic interaction. II, *Philos. Mag.* 33 (1917) 521–533.
- [57] J. Applequist, J.R. Carl, K.-K. Fung, An atom dipole interaction model for molecular polarizability. Application to polyatomic molecules and determination of atom polarizabilities, *J. Am. Chem. Soc.* 94 (1972) 2952–2960.
- [58] E.M. Purcell, C.R. Pennypacker, Scattering and absorption of light by nonspherical dielectric grains, *Astrophys. J.* 1986 (1973) 705–714.
- [59] B.T. Draine, P.J. Flatau, Discrete-dipole approximation for scattering calculations, *J. Opt. Soc. Am. A* 11 (1994) 1491–1499.
- [60] C. Girard, The electronic structure of an atom in the vicinity of a solid body: Application to the physisorption on metal surface, *J. Comput. Phys.* 85 (1986) 6750–6757.
- [61] O.J.F. Martin, C. Girard, A. Dereux, Generalized field propagator pf electromagnetic scattering and light confinement, *Phys. Rev. Lett.* 74 (1995) 526–529.
- [62] M. Devel, C. Girard, C. Joachim, Computation of electrostatic fields in low-symmetry systems: application to STM configurations, *Phys. Rev. B* 53 (1996) 13159–13168.
- [63] C.-T. Tai, Dyadic green functions in electromagnetic theory, *Inst. Electr. Electron. Eng.* (1994).
- [64] F. Torrens, M. Ruiz-Lopez, C. Cativiela, J.I. Garcia, J.A. Mayoral, Conformational aspects of some asymmetric diels-alder reactions. a molecular mechanics + polarization study, *Tetrahedron* 48 (1992) 5209–5218.
- [65] F. Torrens, J. Sanchez-Martin, I. Nebot-Gill, Interacting induced dipoles polarization model for molecular polarizabilities. Reference molecules, *J. Mol. Struct. Theochem.* 463 (1999) 27–39.
- [66] F. Torrens, Polarization force fields for peptides implemented in ecepp2 and mm2, *Mol. Simul.* 24 (2000) 391–400.
- [67] G.A. Kaminski, R.A. Friesner, R. Zhou, A computationally inexpensive modification of the point dipole electrostatic polarization model for molecular simulations, *J. Comput. Chem.* 24 (2003) 267–276.
- [68] F.H. Stillinger, Dynamics and ensemble averages for the polarization models of molecular interactions, *J. Chem. Phys.* 71 (1979) 1647–1651.
- [69] C. Girard, Multipolar propagators near a corrugated surface: implication for local probe microscopy, *Phys. Rev. B* 45 (1992) 1800–1810.
- [70] A.J. Stone, *The Theory of Intermolecular Forces*, Oxford University Press, 1996.
- [71] M.L. Olson, K.R. Sundberg, An atom monopole–dipole interaction model with charge transfer for the treatment of polarizabilities of pi-bonded molecules, *J. Chem. Phys.* 69 (1978) 5400–5404.
- [72] A. Mayer, A monopole–dipole model to compute the polarization of metallic carbon nanotubes, *Appl. Phys. Lett.* 86 (2005) 153110.
- [73] R.B. Birge, Calculation of molecular polarizabilities using an anisotropic point dipole interaction model which includes the effect of electron repulsion, *J. Chem. Phys.* 72 (1980) 5312–5319.
- [74] B.T. Thole, Molecular polarizabilities calculated with a modified dipole interaction, *Chem. Phys.* 59 (1981) 341–350.
- [75] B. Shanker, J. Applequist, Atom monopole–dipole interaction model with limited delocalization length for polarization of polyenes, *J. Phys. Chem.* 100 (1996) 10834–10836.
- [76] L. Jensen, P.-O. Åstrand, K.V. Mikkelsen, An atomic capacitance-polarizability model for the calculation of molecular dipole moments and polarizabilities, *Int. J. Quantum Chem.* 84 (2001) 513–522.

- [77] L. Jensen, P.-O. Åstrand, A. Osted, J. Kongsted, K.V. Mikkelsen, Polarizability of molecular clusters as calculated by a dipole interaction model, *J. Comput. Phys.* 116 (2002) 4001–4010.
- [78] Z. Wang, X. Zu, L. Yang, F. Gao, W.J. Weber, Atomistic simulation of the size orientation and temperature dependence of tensile behavior in GaN nanowires, *Phys. Rev. B* 76 (2007) 045310.
- [79] A. Mayer, Polarization of metallic carbon nanotubes from a model that includes both net charges and dipoles, *Phys. Rev. B* 71 (2005) 235333.
- [80] R. Langlet, M. Devel, P. Lambin, Computation of the static polarizabilities of multi-wall carbon nanotubes and fullerenes using a Gaussian regularized point dipole interaction model, *Carbon* 44 (2006) 2883–2895.
- [81] S.W. de Leeuw, J.W. Perram, E.R. Smith, Simulation of electrostatic systems in periodic boundary conditions. i. lattice sums and dielectric constants, *Proc. R. Soc. Lond. A* 373 (1980) 27–56.
- [82] E. Tadmor, M. Ortiz, R. Phillips, Quasicontinuum analysis of defects in solids, *Philos. Mag. A* 73 (1996) 1529–1563.
- [83] M. Arroyo, T. Belytschko, An atomistic-based finite deformation membrane for single layer crystalline films, *J. Mech. Phys. Solids* 50 (2002) 1941–1977.
- [84] P.A. Klein, A virtual internal bond approach to modeling crack nucleation and growth, Ph.D. Thesis, Stanford University, 1999.
- [85] P. Zhang, Y. Huang, P.H. Geubelle, P.A. Klein, K.C. Hwang, The elastic modulus of single-wall carbon nanotubes: a continuum analysis incorporating interatomic potentials, *Int. J. Solids Struct.* 39 (2002) 3893–3906.
- [86] Z. Tang, H. Zhao, G. Li, N.R. Aluru, Finite-temperature quasicontinuum method for multiscale analysis of silicon nanostructures, *Phys. Rev. B* 74 (2006) 064110.
- [87] D. Wolf, P. Keblinski, S.R. Phillpot, J. Eggebrecht, Exact method for the simulation of coulombic systems by spherically truncated, pairwise r^{-1} summation, *J. Chem. Phys.* 110 (1999) 8254–8282.
- [88] C.J. Fennell, J.D. Gezelter, Is the Ewald summation still necessary? Pairwise alternatives to the accepted standard for long-range electrostatics, *J. Chem. Phys.* 124 (2006) 234104.